

Modality-Aware Triplet Hard Mining for Zero-shot Sketch-Based Image Retrieval

Zongheng Huang¹, Yifan Sun², Chuchu Han¹, Changxin Gao¹, Nong Sang¹

¹Key Laboratory of Ministry of Education for Image Processing and Intelligent Control, School of Artificial Intelligence and Automation, Huazhong University of Science and Technology,

²Baidu Research

{huangzongheng, hcc, cgao, nsang}@hust.edu.cn, sunyf15@tsinghua.org.cn

Abstract

This paper tackles the Zero-Shot Sketch-Based Image Retrieval (ZS-SBIR) problem from the viewpoint of cross-modality metric learning. This task has two characteristics: 1) the zero-shot setting requires a metric space with good within-class compactness and the between-class discrepancy for recognizing the novel classes and 2) the sketch query and the photo gallery are in different modalities. The metric learning viewpoint benefits ZS-SBIR from two aspects. First, it facilitates improvement through recent good practices in deep metric learning (DML). By combining two fundamental learning approaches in DML, e.g., classification training and pairwise training, we set up a strong baseline for ZS-SBIR. Without bells and whistles, this baseline achieves competitive retrieval accuracy. Second, it provides an insight that properly suppressing the modality gap is critical. To this end, we design a novel method named Modality-Aware Triplet Hard Mining (MATHM). MATHM enhances the baseline with three types of pairwise learning, e.g., a cross-modality sample pair, a within-modality sample pair, and their combination. We also design an adaptive weighting method to balance these three components during training dynamically. Experimental results confirm that MATHM brings another round of significant improvement based on the strong baseline and sets up new state-of-the-art performance. For example, on the TU-Berlin dataset, we achieve 47.88+2.94% mAP@all and 58.28+2.34% Prec@100. Code will be publicly available.

1. Introduction

Sketch-Based Image Retrieval (SBIR) aims to retrieve the image-of-interest in the database, using a hand-drawn sketch as the query. It allows searching without image queries and brings great convenience to potential users. The conventional SBIR requires that the training and testing set

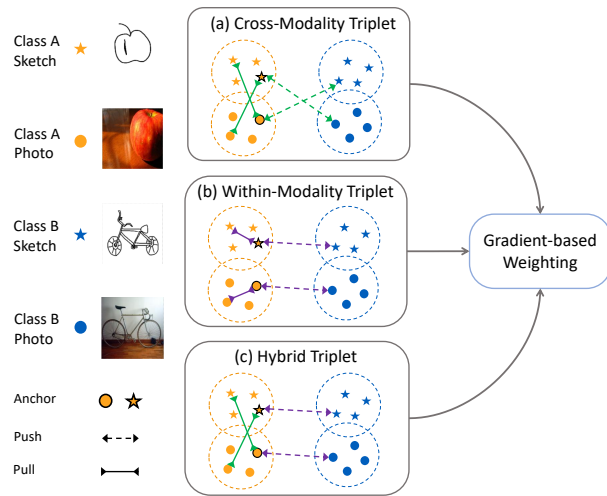


Figure 1. An illustration of three types of triplets. (a) positive and negative images have modalities from the anchor image; (b) positive and negative images have the same modality as the anchor image; (c) positive images have different modalities from the anchor image, and negative images have the same modality as the anchor image. In contrary to the baseline using only (a) triplets, the proposed MATHM dynamically integrates all the three types of triplets through a novel gradient-based weighting strategy.

share the same categories, which limits its real-world applications. In this paper, we consider a more realistic and challenging setting named Zero-Shot SBIR (ZS-SBIR), where all categories of the testing set have not appeared in the training set.

ZS-SBIR can be viewed as a specified cross-modality metric learning task. In such a task, we consider there are two challenges. 1) *Learning a metric space with category discrimination*. Specifically, the zero-shot setting is popular in a series of metric learning applications, e.g., fine-grained image retrieval [40, 41, 63], face recognition [5, 27, 44, 49, 51–53], person re-identification [12, 17, 48]

and vehicle re-identification [2, 23]. In all these tasks, there is no class intersection between the training and testing set, which is consistent with the zero-shot setting. The keynote of these tasks is to learn a metric space in which all the instances from the same class are close and different classes are far away from each other. Such within-class compactness and the between-class discrepancy are vital for the discriminative ability of the novel classes. 2) *Suppressing the modality gap between the sketch query and the photo gallery.* Specifically, the query sketches and gallery images belong to different modalities. The hand-drawn sketch usually contains only the object contour that indicates the primary structure. The details are either neglected or distorted. In contrast, real photos include rich texture and color information. This significant modality gap compromises the within-class compactness, which brings the difficulty of building an accurate metric space.

In response to these two challenges, we tackle the ZS-SBIR problem with metric learning techniques from the following two aspects:

- *First, we set up a strong baseline for ZS-SBIR with recent good practices in deep metric learning (DML) to enhance the category discrimination of feature embedding.* There are two fundamental deep metric learning approaches [5, 30, 47], *e.g.*, classification training and pairwise training. Specifically, the former learns a deep classifier on the training set, encouraging the model to produce class discriminative deep embedding for feature representation. We note that prior works [3, 6, 26, 29, 58, 65, 66] in ZS-SBIR mainly adopt this learning manner. In contrast, the latter directly compares the features against each other in a pairwise manner. A popular implementation is to construct the feature triplet consisting of an anchor, a positive, and a negative feature. The anchor tries to pull the positive feature close and push the negative feature far away. By adding an additional margin to the feature triplets [17], the between-class discrepancy of the learned deep embedding is further enlarged.

Combining these two fundamental training manners with slight task-specific modification, we set up a strong baseline for ZS-SBIR. In the baseline, we naturally modify the “Pos-Anchor-Neg” triplet into “photo-sketch-photo” form (“P^P-A^S-N^P” for simplicity) to meet the objective of the ZS-SBIR task, as shown in Figure 1 (a). Without any bells and whistles, it achieves retrieval accuracy on par with the state-of-the-art. We believe the simplicity and competitive performance will allow it to serve as a strong baseline for the ZS-SBIR community.

- *Second, we propose a novel method named Modality-Aware Triplet Hard Mining (MATHM) to suppress the modality gap between the sketch query and the photo gallery.* Based on the baseline, MATHM further narrows the modality gap by supplementing the baseline with two

other triplet forms, *e.g.*, the “P^S-A^S-N^S” and “P^P-A^S-N^S” triplets, as illustrated in Figure 1 (b) and (c), respectively. The “P^S-A^S-N^S” enforces category discrimination under a single modality, while the “P^P-A^S-N^S” triplet explicitly suppresses the modality gap. Moreover, we design an adaptive weighting scheme to balance these triplets during training dynamically. In Section 4.4, we reveal an important superiority of the proposed MATHM, *i.e.*, it suppresses the modality gap without decreasing the between-class discrepancy within every single modality.

The contributions are summarized as follows:

- We construct a simple yet strong baseline for the ZS-SBIR task by combining two fundamental deep metric learning methods. Without bells and whistles, the performance of our baseline is on par with recent works.
- We propose a novel method named Modality-Aware Triplet Hard Mining, which further narrows the modality gap with three types of pair-wise learning. Meanwhile, an adaptive weighting strategy is developed to balance the three components.
- We evaluate our proposed MATHM on two SBIR datasets. It surpasses the previously best methods and sets new state-of-the-art.

2. Related Works

2.1. Deep Metric Learning

Deep Metric Learning aims to map the input images from the pixel space to the embedding space with a deep Convolutional Neural Network (CNN), where images of the same class are close, and images of different classes are far away from each other. Typically, an embedding loss or a classification loss is adopted to manipulate the features in the embedding space to achieve good within-class compactness and the between-class discrepancy. The embedding loss usually focuses on mining the relationship among image pairs or triplets by enforcing a margin between positive and negative pairs in the embedding space, *e.g.* Contrastive Loss [15], Triplet Loss [17, 44, 56], Lifted-Structure loss [34], Angular loss [54], N-Pair Loss [46], Multi-Similarity Loss [55], and FastAP [1]. And the classification loss utilizes a weight matrix as learnable class centers to exploit the global relationship between each sample to all categories, *e.g.* Softmax Loss [36, 49], NormFace [52], SphereFace [27], CosFace [51, 53], ArcFace [5], SoftTriplet Loss [39], ProxyNCA [33], and *etc.*

As each category contains both sketch and photo images, the data distribution for the SBIR task is multi-modal. While most classification losses require that the data distribution is uni-modal (except for the SoftTriplet Loss, which uses multiple class centers), we select the more flexible

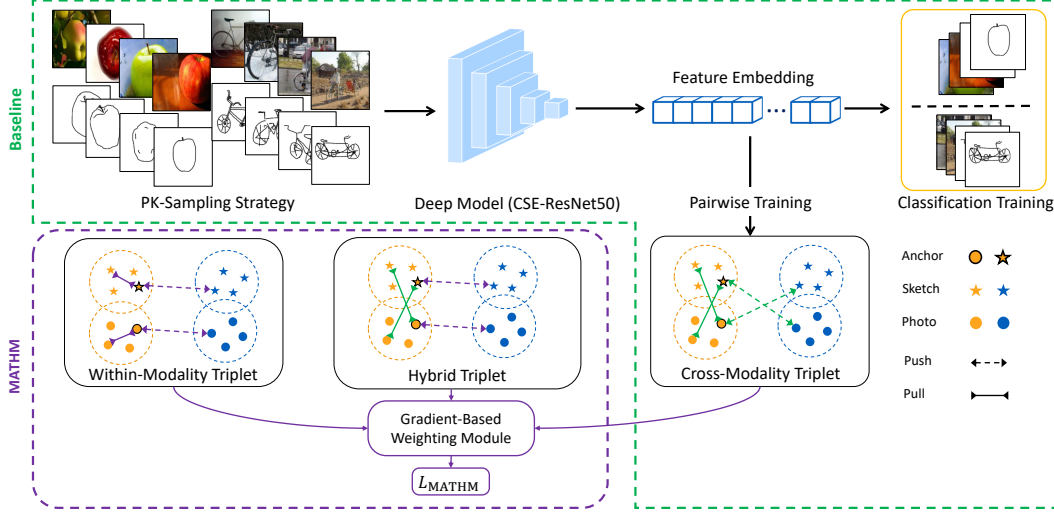


Figure 2. An overview of the proposed ZS-SBIR baseline, as well as the novel MATHM method. The **Baseline** combines two fundamental training approaches, *e.g.*, classification training and pairwise training for supervision. Since ZS-SBIR aims to retrieve photos according to the sketch query, the pairwise training uses the sketch as the anchor and selects the furthest positive and closest negative photos to construct a cross-modality triplet. Based on this baseline, **MATHM** supplements the cross-modality triplet with two other forms of triplet (within-modality triplet and hybrid triplet), as well as a gradient-based weighting module. Learning from the within-modality triplet enhances the category discrimination under every single modality while learning from the hybrid triplet directly suppresses the modality gap. All three types of triplet loss are dynamically aggregated with the gradient-based weighting module to calculate the overall embedding loss.

triplet embedding loss to train our model, for it puts no restriction on the prior data distribution.

2.2. SBIR and ZS-SBIR

The main challenge of the SBIR task is the modality discrepancy between hand-drawn sketches and real photos. Earlier works often use edge maps [64] extracted from real images as mid-level representation to bridge the gap between photos and sketches. Some specially designed feature descriptors, *e.g.* Bag Of Words (BOG) [10, 11], HOG [19], Learned KeyShapes (LKS) [42], are used to represent the sketches and edge-maps simultaneously. In recent years, many deep learning-based methods have emerged [25, 29, 43, 59–62]. These methods train a CNN end-to-end to map the sketches and photo images into a shared embedding space.

However, traditional SBIR methods assume that the training and testing set share the same categories, which is inapplicable to real-life scenarios. [45] proposes a more realistic setting named Zero-Shot Sketch-Based Image Retrieval (ZS-SBIR), where the testing classes are unseen during training. A majority of works on ZS-SBIR leverage semantic information obtained from language models [20, 31, 32, 38] to encourage knowledge transfer to unseen classes. To achieve this, [35] uses a stacked adversarial network to align features from different modalities; [6, 57, 58, 66] combine the generative adversarial network with the auto-encoder to encode the visual feature and se-

mantic feature to common space; [45, 65] utilize graph neural network to fuse the semantic information with visual representation.

3. Methodology

In this section, we start with introducing our metric learning baseline for ZS-SBIR, then describe our Modality-Aware Triplet Hard Mining strategy and the gradient-based weighting scheme.

3.1. The Metric Learning Baseline

3.1.1 Two Fundamental Training Approaches

Let $X = \{(x_i^m, y_i) | y_i \in C, m \in \{s, p\}\}_{i=1}^N$ be the training set (s denotes sketch while p denotes photo), where x_i^m is an image with label y_i from modality m and C is the training class set. The distance function $D(x_i^{m_1}, x_j^{m_2}) = \|f_\theta(x_i^{m_1}) - f_\theta(x_j^{m_2})\|_2$ calculates the Euclidean distance between an image pair. $f_\theta(\cdot)$ is the embedding function that is parameterized by θ , which maps the images into a L2-normalized embedding space.

Following the common practice in deep metric learning, a triplet embedding loss is combined with a softmax cross-entropy classification loss to form our baseline. The learning objective is formulated as:

$$\mathcal{L}_{all} = \mathcal{L}_{cls} + \lambda \mathcal{L}_{cross}, \quad (1)$$

where \mathcal{L}_{cls} is the classification loss, and \mathcal{L}_{cross} is the embedding loss. λ is a hyper-parameter that controls the relative weight of the two kinds of losses. An overview of our baseline is shown in Figure 2.

Classification Training. The primary target of the classification training in this task is to stabilize the training process. We can optimize our model from a global level with a classification loss since it uses a weight matrix to store the proxies for all categories. In contrast, the pairwise training focuses on the relationship among a small subset of classes within the current mini-batch. Thus our model will likely be trapped in a bad local optimum if trained without the classification loss. The standard softmax cross-entropy loss is adopted for classification training, which is defined as:

$$\mathcal{L}_{cls} = -\log \frac{e^{W_{y_i}^T \cdot f(x_i^m)}}{\sum_{c \in C} e^{W_c^T \cdot f(x_i^m)}}, \quad (2)$$

where W_c is the weight term in the classifier Θ_C corresponding to category c .

Pairwise Training. Distinct from the traditional single modality image retrieval problems, the query sketches and the gallery images are from different modalities in the ZS-SBIR task. We expect that for any anchor sketch image x_a^s , its positive photo image x_i^p should be closer to x_a^s than its negative photo image x_j^p in the embedding space:

$$D(x_a^s, x_i^p) < D(x_a^s, x_j^p), y_a = y_i \neq y_j. \quad (3)$$

To achieve the above goal, we design a cross-modality triplet loss to directly reduce $D(x_a^s, x_i^p)$ and increase $D(x_a^s, x_j^p)$. One of the key issues of SBIR is to resolve the discrepancy between sketch and photo. Thus, it is vital to maintain a consistency scheme: if the photo closest to sketch s is p , we hope that the sketch closest to photo p is also s . So both sketch and photo are selected as anchors to form cross-modality triplets. The cross-modality triplet loss is then defined as:

$$\mathcal{L}_{cross} = [(D(x_a^s, x_i^p)) - D(x_a^s, x_j^p) + \alpha]_+ + [(D(x_a^p, x_i^s)) - D(x_a^p, x_j^s) + \alpha]_+, \quad (4)$$

where the x_a and x_i are from the same category, while the x_a and x_j are from different categories. A positive margin parameter α is added for better separability in the embedding space for different categories.

3.1.2 Sampling Strategy

Following the conventional PK sampling strategy [17], we form a mini-batch by randomly sample P classes and then

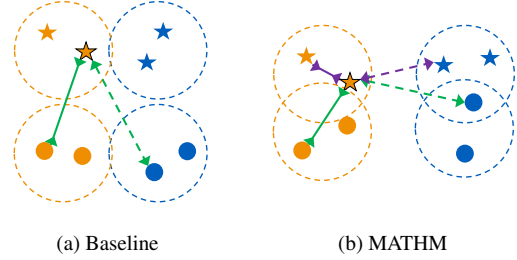


Figure 3. (a) Our baseline has high tolerance on the modality gap, where the gap hurts within-class compactness in the testing phase and deteriorates the model’s performance for the ZS-SBIR task. (b) In order to obtain better within-class compactness, we not only impose baseline constraints but also explicitly suppress the modality gap with the MATHM. Each color represents a particular class. The stars denote sketches, and circles denote photos. Best viewed in color.

sample K images of each modality from each category. Thus the total batch size is $2 \times PK$. For each sample in the mini-batch, we select the hardest positive and hardest negative from the corresponding modality within the mini-batch to form a triplet T :

$$\begin{cases} T = (x_a^{m_a}, x_{pos}^{m_p}, x_{neg}^{m_n}) \\ pos = \arg \max_i D(x_a^{m_a}, x_i^{m_p}), & y_a = y_i \\ neg = \arg \min_j D(x_a^{m_a}, x_j^{m_n}), & y_a \neq y_j \end{cases} \quad (5)$$

where m_a, m_p, m_n stand for the modality of the anchor, positive, and negative images, respectively. For our cross-modality triplet loss, we have $m_a \neq m_p = m_n$, which means that we only select positive and negative images with different modalities from the anchor image to form a triplet.

3.1.3 Network Architecture

We adopt a single stream CNN as the feature extractor to map images from different modalities to a shared embedding space. Following [26], we select CSE-ResNet50 [29] as our backbone model. The CSE-ResNet50 integrates the conditional SE module into ResBlocks [16], which effectively handles inputs from different modalities.

3.2. Modality-Aware Triplet Hard Mining

Our Modality-Aware Triplet Hard Mining aims at utilizing hard triplets of different modal compositions to train a robust ZS-SBIR model.

For the SBIR problem, the distance between the query sketches and gallery photos is related to both the class level discrepancy and the modality gap. Assuming that the distance between two images $d_{i,j} = D(x_i^{m_i}, x_j^{m_j})$ can be decomposed into two parts:

$$d_{i,j} = G(d_{i,j}^c, d_{i,j}^m), \quad (6)$$

where G is an abstract function that aggregates the class-specific distance $d_{i,j}^c$ and the modality-specific distance $d_{i,j}^m$. The cross-modality triplet loss optimizes the overall distance $d_{i,j}$ on cross-modality triplets, which neither explicitly reduces the modality gap nor ensures that the within-class distance is smaller than the between-class distance. As the example shown in Figure 3, although the cross-modality triplet loss has been satisfied, the modality gap and within-class variation are still large. To train a strong cross-modality embedding function, we need to reduce the modality gap and make each testing class separable from the other. Therefore, we extend our baseline with two other triplet relationships, *e.g.*, the within-modality triplet relationship and hybrid triplet relationship. The standard triplet embedding loss with batch-hard triplet mining (Eq. (5)) is used for loss calculation, detailed as follows.

Within-Modality Triplet. This is a typical triplet relationship in single modal metric learning tasks. The positive and negative images with the same modality as the anchor image ($m_a = m_n = m_p$) are selected to form a triplet for learning discriminative embedding within each modality. The within-modal triplet loss is defined as:

$$\mathcal{L}_{in} = [(D(x_a^s, x_i^s)) - D(x_a^s, x_j^s) + \alpha]_+ + [(D(x_a^p, x_i^p)) - D(x_a^p, x_j^p) + \alpha]_+. \quad (7)$$

The above loss function encourages our model to learn a class discriminative feature embedding for input sketches and photos. Since no cross-modality relationship is included, using the within-modality triplet loss alone is less effective to handle this cross-modality matching problem.

Hybrid Triplet. Modality gap is a major concern in the cross-modality matching tasks. One of the common solutions to this problem is to align the feature distribution of two modalities using the Generative Adversarial Mechanism [14]. The learned feature embedding for sketches and photos is expected to be similar enough to “fool” the discriminator, thus the modality gap is minimized. However, reducing the modality gap is not the only challenge for the SBIR problem, learning discriminative feature embedding is also of vital importance. Due to the large inherent differences between sketches and photos, directly narrowing the modality gap might weaken the expressiveness of feature embedding and further compromise the performance of SBIR. Thus we design the hybrid triplet loss to tackle the modality discrepancy problem while preserving the between-class discrepancy.

The hybrid triplet is composed of an anchor image, a cross-modality positive image, and a same-modality negative image ($m_a = m_n \neq m_p$). The corresponding loss function is written as:



Figure 4. The changes in gradient during training.

$$\mathcal{L}_{hyb} = [(D(x_a^s, x_i^p)) - D(x_a^s, x_j^s) + \alpha]_+ + [(D(x_a^p, x_i^s)) - D(x_a^p, x_j^p) + \alpha]_+. \quad (8)$$

The above loss function aims to minimize the distance between cross-modality positives and maximizes that of the same modality negatives. The pull term minimizes the modality gap $d_{a,i}^m$ and the within-class variation $d_{a,i}^c$ concurrently, while the push term maximizes the between-class discrepancy. Therefore, the hybrid triplet loss is capable of suppressing the modality gap while maintaining the between-class discrepancy. We will experimentally validate this assumption in Section 4.4.

3.3. Gradient-based Weighting Scheme

We will first briefly revisit the gradient calculation of triplet loss and then introduce our gradient-based weighting scheme for aggregating different triplet losses. The general form of triplet embedding loss is formulated as:

$$\mathcal{L}_i = \frac{1}{N} \sum [d_{ap} - d_{an} + \alpha]_+, \quad (9)$$

where $[\bullet + \alpha]_+$ is the hinge function. The above equation implies that only the triplets with a positive value in $(d_{ap} - d_{an} + \alpha)$ will produce gradients for optimization. The gradient g_i w.r.t. \mathcal{L}_i is calculated as:

$$g_i = \frac{1}{N} \sum \text{sgn}([d_{ap} - d_{an} + \alpha]_+). \quad (10)$$

As each of the three triplet losses plays an essential role in learning a good embedding, we prefer that they could contribute equally in the training stage. One typical way to integrate multiple loss functions is by summation, but it is not optimal. The contribution of each loss function depends on the gradient they produced during the backward pass. But the gradient of each triplet loss decays at varying speeds due to their different convergence targets (as Figure 4 shows). Some of them are hard to converge, for which they consistently produce strong gradients. This phenomenon indicates that the harder ones will dominate

Table 1. The performance comparison of MATHM and existing methods on ZS-SBIR tasks. “†” denotes experiments using binary hashing codes. The rest use real-valued features. ITQ [13] is used to binarize our feature to compare with the zero-shot hashing methods. The best results are in **bold**, while the best results of previous methods are in **blue**.

Task	Method	dim	TU-Berlin Ext.		Sketchy Ext.		Sketchy Ext.([58] Split)	
			mAP@all	Prec@100	mAP@all	Prec@100	mAP@200	Prec@200
SBIR	GN-triplet [43]	1024	18.9	24.1	21.1	31.0	8.3	16.9
	DSH [25]	64†	12.2	19.8	16.4	22.7	5.9	15.3
ZSL	SAE [22]	300	16.1	21.0	21.0	30.2	13.6	23.8
	ZSH [57]	64	13.9	17.4	16.5	21.7	-	-
ZS-SBIR	ZSIH [45]	64	22.0	29.1	25.4	34.0	-	-
	EMS [29]	512	25.9	36.9	-	-	-	-
		64	16.5	25.2	-	-	-	-
	CCAIE [58]	4096	-	-	19.6	28.4	15.6	26.0
		64	29.7	42.6	34.9	46.3	-	-
	SEM-PCYC [7]	64†	29.3	39.2	34.4	39.9	-	-
		512	47.5	59.9	54.7	69.2	49.7	59.8
	SAKE [26]	64†	35.9	48.1	36.4	48.7	35.6	47.7
	SketchGCN [65]	1024	32.4	50.5	38.2	53.8	-	-
	Doodle2Search [6]	4096	10.9	-	36.9	-	-	-
	STYLE-GUIDE [8]	4096	25.4	35.6	37.6	48.4	35.8	40.0
	BDT [24]	1024	-	-	-	-	28.1	39.4
	OCEAN [66]	512	33.3	46.7	46.2	59.0	-	-
	PCMSN [3]	64	42.4	51.7	52.3	61.6	-	-
		64†	35.5	45.2	50.6	61.5	-	-
	Baseline (ours)	512	47.88 ± 0.07	58.28 ± 0.14	58.72 ± 0.42	70.26 ± 0.42	48.78 ± 0.21	60.06 ± 0.25
		64†	39.76 ± 0.28	50.72 ± 0.12	49.72 ± 0.43	63.28 ± 0.28	45.08 ± 0.36	54.32 ± 0.31
	MATHM (ours)	512	50.82 ± 0.12	60.62 ± 0.18	62.92 ± 0.14	73.80 ± 0.11	52.26 ± 0.11	63.28 ± 0.20
	64†	42.94 ± 0.58	54.06 ± 0.47	55.36 ± 0.60	66.00 ± 0.43	47.78 ± 0.57	57.58 ± 0.46	

the optimization if we aggregate these losses by summation. Thus we design a gradient-based weighting scheme to make equal use of all these losses. Assume the values of the above loss functions (Eq. (4, 7, 8)) at the current iteration are $\mathcal{L}_i (i = 1, 2, 3)$, where the gradient *w.r.t.* \mathcal{L}_i is g_i , and the weight of \mathcal{L}_i is w_i . We gather the three components of MATHM with the gradient-based weighting scheme to form the overall embedding loss:

$$\mathcal{L}_{\text{MATHM}} = \sum_{i=1}^n w_i \mathcal{L}_i. \quad (11)$$

The $\mathcal{L}_{\text{cross}}$ in Eq. (1) is replaced with $\mathcal{L}_{\text{MATHM}}$ to form our total learning objective.

Our goal is to ensure that each loss function produces an equal amount of gradient. Meanwhile, the total magnitude of gradients should remain the same after weighting. This objective can be formulated as:

$$\begin{cases} w_i g_i = w_j g_j, & \forall i \neq j \\ \sum_{i=1}^n w_i g_i = \sum_{i=1}^n g_i \end{cases} \quad (12)$$

We solve the above equation set to calculate w_i :

$$w_i = \frac{1}{n} \sum_{k=1}^n \frac{g_k}{g_i}, \quad (13)$$

where n equals to 3 in this case.

The gradient-based weighting scheme ensures that each loss function produces an equal magnitude of gradients in every step, reasonably aggregating the three triplet losses.

4. Experimental Results

4.1. Datasets and Setup

We evaluate our model on two popular large-scale SBIR benchmarks: the TU-Berlin [9] Extended and the Sketchy [43] Extended.

TU-Berlin Extended contains 20,000 sketch images of 250 categories from the TU-Berlin dataset and 204,489 extra photo images from [61]. Following [45], we choose 30 identical classes as the unseen set while the other 220 categories are used for training.

Sketchy Extended originally contains 12,500 photo images and 75,479 sketch images from 125 different classes. [25] extended this dataset by adding 60,502 natural images to the photo domain, so the total number of photo images is 73,002. [45] propose a zero-shot evaluation protocol by randomly chosen 25 categories as the unseen set. But [58] suggests that some randomly chosen categories in the unseen set might have appeared in the ImageNet [4], which violates the zero-shot assumption when using the ImageNet pre-trained weights for model initialization. Therefore they

Table 2. The quantitative analysis of the proposed methods and the generative adversarial network on the TU-Berlin testing set. \uparrow means the larger the better and \downarrow means the smaller the better. The best results are in bold. The confidence intervals are omitted for clarity.

Methods	Similarity	Within-Class	Between-Class	Within-Class Modality gap \downarrow	Between-Class Discrepancy		mAP@all \uparrow	Prec@100 \uparrow
					Same-Modality \uparrow	Cross-Modality \uparrow		
Baseline	Same-Modality	0.527	0.070	0.259	0.456	0.224	47.88	58.28
	Cross-Modality	0.268	0.044					
MATHM	Same-Modality	0.531	0.129	0.158	0.402	0.247	50.82	60.62
	Cross-Modality	0.373	0.126					
GAN	Same-Modality	0.653	0.368	0.072	0.285	0.218	40.19	56.81
	Cross-Modality	0.581	0.363					

put forward a new protocol using 21 carefully selected categories orthogonal to the ImageNet classes as the unseen set. We will conduct our experiments under both of these two protocols to validate our method.

4.2. Implementation details

We implement our method using PyTorch [37] toolbox with one RTX2080Ti GPU. An ImageNet pre-trained SE-ResNet50 [18] is used to initialize our model. We use Adam [21] optimizer with parameter $\beta_1 = 0.9$, $\beta_2 = 0.999$ to train our model. The margin parameter α in all our triplet losses is set to 0.2. The initial learning rate is set to $1e-4$, and cosinely [28] decays to zero during training. For all the pre-trained layers, the learning rate is set to $0.1 \times$ the base learning rate. The batch size is set to 128, where the number of classes $P = 16$ and the number of images per class $K = 4$ for our sampler. The whole network is trained for 8000 iterations to converge. We do five training runs in all our experiments and report the average of mean Average Precision (mAP@all) and Precision (Prec@100), as well as the 95% confidence intervals.

4.3. Comparison with the State-of-the-Art

We compare our methods with several existing works on ZS-SBIR. Most of them use semantic information. The earlier works such as ZSIH [45], CCAE, CVAE [58], Doodle2Search [6] use a relatively simple framework, which adopts a single auto-encoder or reconstruction loss to combine semantic information with the visual feature. Recent works like OCEAN [66], SketchGCN [65], PCMSN [3] and SEM-PCYC [7] use more complicated structures. They combine multiple generative adversarial networks or graph neural networks with auto-encoder for learning a shared visual-semantic embedding space. Another recent work, SAKE [26], designs a teacher-student architecture for learning semantic information while preserving the pre-trained knowledge from ImageNet. We also compare our methods with another metric learning approach, EMS [29], which enforces a class-level margin in the euclidean embedding space by using the Euclidean Margin Softmax (EMS) as the classification loss.

As Table 1 shows, our simple baseline surpasses most of the existing methods. MATHM further improves the

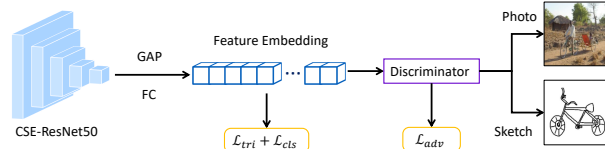


Figure 5. Network architecture for the generative adversarial network.

retrieval accuracy and outperforms all the state-of-the-art methods by a large margin. Compared with one previous classification loss EMS, our triplet-based embedding losses show a significant performance boost. The competitive performance of our approach demonstrates that pairwise training is more effective than classification training under the cross-modality setting.

4.4. Effect of MATHM

We will experimentally validate the effectiveness of MATHM by comparing it with another popular feature alignment method: the **Generative Adversarial Network** (GAN). As Figure 5 shows, we build up the GAN based on our baseline: we add a fully connected layer after the embedding layer as the discriminator D and use all the other parts of our baseline as the generator G . Given an input sample, the generator G tries to conceal the actual modality in the deep feature space, while the discriminator tries to distinguish whether the feature is generated from a sketch or a real photo. Thus the generator tends to produce features that have similar distribution for input sketches and photos. The detailed implementation of GAN is described in Appendix A.1.

Section 3.2 points out that the model’s performance on SBIR task is closely related to two properties of the embedding space: 1) the modality gap and 2) the between-class discrepancy. In this paragraph, we will figure out how generative adversarial training and MATHM affect the model’s performance on SBIR. We make a quantitative analysis of the modality gap by calculating the mean difference between the average cosine similarity of same-modality and cross-modality samples of each testing class. And the between-class discrepancy is measured by the mean difference of the average cosine similarity of same-class samples and different-class samples on the testing set.

Table 3. Analysis on each component of the proposed method.

\mathcal{L}_{cross}	\mathcal{L}_{in}	\mathcal{L}_{hyb}	GW	TU-Berlin Ext.		Sketchy Ext.		Sketchy Ext. ([58] Split)	
				mAP@all	Prec@100	mAP@all	Prec@100	mAP@200	Prec@200
				46.00 \pm 0.16	56.42 \pm 0.18	54.40 \pm 0.21	66.02 \pm 0.27	45.94 \pm 0.11	57.70 \pm 0.18
✓				47.88 \pm 0.07	58.28 \pm 0.14	58.72 \pm 0.42	70.26 \pm 0.42	48.78 \pm 0.21	60.06 \pm 0.25
	✓			47.58 \pm 0.21	57.78 \pm 0.13	57.44 \pm 0.31	68.68 \pm 0.31	48.58 \pm 0.21	60.56 \pm 0.29
		✓		48.78 \pm 0.27	58.88 \pm 0.31	59.36 \pm 0.39	70.96 \pm 0.38	49.52 \pm 0.07	61.06 \pm 0.10
✓	✓			48.97 \pm 0.34	59.17 \pm 0.22	60.50 \pm 0.18	72.70 \pm 0.19	51.16 \pm 0.16	62.94 \pm 0.21
✓		✓		49.12 \pm 0.16	59.36 \pm 0.13	61.14 \pm 0.30	72.98 \pm 0.19	51.70 \pm 0.13	63.50 \pm 0.24
✓	✓	✓		50.40 \pm 0.14	60.28 \pm 0.08	62.20 \pm 0.11	73.20 \pm 0.07	51.84 \pm 0.14	62.72 \pm 0.12
✓	✓	✓	✓	50.82 \pm 0.12	60.62 \pm 0.18	62.92 \pm 0.14	73.80 \pm 0.11	52.26 \pm 0.11	63.28 \pm 0.20

As results shown in Table 2, the GAN achieves the best performance on reducing the modality gap between the same class samples, but it performs worst on enlarging the between-class discrepancy for both the same-modality and cross-modality samples. For which it gets the lowest mAP and Precision on the SBIR benchmark. Our baseline performed slightly better than others on the between-class discrepancy for same-modality samples, but it has the largest modality gap, which compromises its performance on SBIR. In contrast, the proposed MATHM performs reasonably well on reducing the modality gap as well as enlarging the between-class discrepancy, achieving the best performance on the SBIR benchmarks. This again validates that reducing the modality gap and enlarging the between-class discrepancy is of equal importance for the SBIR task.

4.5. Ablation Study

In this section, we will focus on evaluating the effectiveness of each component of our method. The experimental results are shown in Table 3, where the \mathcal{L}_{cross} , \mathcal{L}_{in} , and \mathcal{L}_{hyb} stand for the cross-modality triplet loss, within-modality triplet loss, and hybrid triplet loss, respectively. *GW* denotes using a gradient-based weighting strategy to aggregate the used embedding loss.

To validate the effectiveness of each components, we first train a model to map the sketches and photos into a common embedding space with only the classification loss. Then we enhance the model with the cross-modality triplet loss, within-modality triplet loss and the hybrid triplet loss separately. The results shows that each type of triplet loss improves the mAP and Prec scores by a different margin. The within-modality triplet loss performs slightly worse than the baseline cross-modality triplet loss, while the hybrid triplet loss performs better than our baseline. This implies that the cross-modality relationship is more important than the within-modality relationship in the ZS-SBIR task. But using the two types of relationships separately could not lead to optimal performance. Next, we combine our baseline with the other two types of triplet loss (the within-modality triplet loss and hybrid triplet loss). The combination of all three triplet losses significantly outperforms our baseline, while combine the baseline with the within-

modality triplet loss and hybrid triplet loss separately only brings marginal improvement. This experiment confirms that the within-modality triplet loss and hybrid triplet loss complement each other. Missing either one of them will greatly deteriorate the performance. Finally, we introduce the gradient-based weighting scheme to our model for aggregating all these losses, which further improves the retrieval accuracy. The above experiments validate that each of the three triplet losses, as well as the weighting strategy, are indispensable for training a strong ZS-SBIR model.

The analysis of hyper-parameter λ and qualitative analysis of MATHM are included in the supplementary material for the limited space.

5. Limitations

In MATHM, we implicitly assumed that the sketches and photos from the same category should be visually similar. A shared CNN backbone is capable of capturing their visual similarity. The visualization of retrieval in Appendix A.3 shows that our model can correctly retrieve visually similar images to the query sketch but might produce wrong results for some ambiguous inputs, *e.g.*, the sketch of objects with similar contour but different texture or color. How to deal with the ambiguity of the hand-drawn sketches will be explored in our future work.

6. Conclusion

This paper tackles the ZS-SBIR task and makes two contributions. First, we integrate two popular deep metric learning manners, *i.e.*, the classification learning and pairwise learning, to learn a discriminative metric space. It achieves competitive retrieval accuracy without bells and whistles, providing a simple and strong baseline for ZS-SBIR. Second, based on this baseline, we further suppress the modality gap of sketch query and photo gallery using a novel Modality-Aware Triplet Hard Mining (MATHM) method. MATHM enhances the baseline (particularly the pairwise training part) with several triplet forms, namely within-modality triplet and hybrid triplet. By dynamically balancing the contribution of these triplets during training, MATHM effectively suppresses the modality gap and facili-

tates better category discrimination. Extensive experiments conducted on TU-Berlin and Sketchy validate the effectiveness of MATHM. The achieved results are on par with the state-of-the-art.

References

- [1] Fatih Cakir, Kun He, Xide Xia, Brian Kulis, and Stan Sclaroff. Deep metric learning to rank. In *Proceedings of the IEEE/CVF Conference on Computer Vision and Pattern Recognition*, pages 1861–1870, 2019. 2
- [2] Ruihang Chu, Yifan Sun, Yadong Li, Zheng Liu, Chi Zhang, and Yichen Wei. Vehicle re-identification with viewpoint-aware metric learning. In *Proceedings of the IEEE/CVF International Conference on Computer Vision*, pages 8282–8291, 2019. 2
- [3] Cheng Deng, Xinxun Xu, Hao Wang, Muli Yang, and Dacheng Tao. Progressive cross-modal semantic network for zero-shot sketch-based image retrieval. *IEEE Transactions on Image Processing*, 29:8892–8902, 2020. 2, 6, 7
- [4] Jia Deng, Wei Dong, Richard Socher, Li-Jia Li, Kai Li, and Li Fei-Fei. Imagenet: A large-scale hierarchical image database. In *2009 IEEE conference on computer vision and pattern recognition*, pages 248–255. Ieee, 2009. 6
- [5] Jiankang Deng, Jia Guo, Niannan Xue, and Stefanos Zafeiriou. Arcface: Additive angular margin loss for deep face recognition. In *Proceedings of the IEEE/CVF Conference on Computer Vision and Pattern Recognition*, pages 4690–4699, 2019. 1, 2
- [6] Sounak Dey, Pau Riba, Anjan Dutta, Josep Lladós, and Yi-Zhe Song. Doodle to search: Practical zero-shot sketch-based image retrieval. In *Proceedings of the IEEE/CVF Conference on Computer Vision and Pattern Recognition*, pages 2179–2188, 2019. 2, 3, 6, 7
- [7] Anjan Dutta and Zeynep Akata. Semantically tied paired cycle consistency for zero-shot sketch-based image retrieval. In *Proceedings of the IEEE/CVF Conference on Computer Vision and Pattern Recognition*, pages 5089–5098, 2019. 6, 7
- [8] Titir Dutta and Soma Biswas. Style-guided zero-shot sketch-based image retrieval. In *BMVC*, volume 2, page 9, 2019. 6
- [9] Mathias Eitz, James Hays, and Marc Alexa. How do humans sketch objects? *ACM Transactions on graphics (TOG)*, 31(4):1–10, 2012. 6
- [10] Mathias Eitz, Kristian Hildebrand, Tamy Boubekeur, and Marc Alexa. An evaluation of descriptors for large-scale image retrieval from sketched feature lines. *Computers & Graphics*, 34(5):482–498, 2010. 3
- [11] Mathias Eitz, Kristian Hildebrand, Tamy Boubekeur, and Marc Alexa. Sketch-based image retrieval: Benchmark and bag-of-features descriptors. *IEEE transactions on visualization and computer graphics*, 17(11):1624–1636, 2010. 3
- [12] Xing Fan, Wei Jiang, Hao Luo, and Mengjuan Fei. Sphered: Deep hypersphere manifold embedding for person re-identification. *Journal of Visual Communication and Image Representation*, 60:51–58, 2019. 1
- [13] Yunchao Gong, Svetlana Lazebnik, Albert Gordo, and Florent Perronnin. Iterative quantization: A procrustean approach to learning binary codes for large-scale image retrieval. *IEEE transactions on pattern analysis and machine intelligence*, 35(12):2916–2929, 2012. 6
- [14] Ian J. Goodfellow, Jean Pouget-Abadie, Mehdi Mirza, Bing Xu, David Warde-Farley, Sherjil Ozair, Aaron C. Courville, and Yoshua Bengio. Generative adversarial networks. *Commun. ACM*, 63(11):139–144, 2020. 5
- [15] Raia Hadsell, Sumit Chopra, and Yann LeCun. Dimensionality reduction by learning an invariant mapping. In *2006 IEEE Computer Society Conference on Computer Vision and Pattern Recognition (CVPR'06)*, volume 2, pages 1735–1742. IEEE, 2006. 2
- [16] Kaiming He, Xiangyu Zhang, Shaoqing Ren, and Jian Sun. Deep residual learning for image recognition. In *Proceedings of the IEEE conference on computer vision and pattern recognition*, pages 770–778, 2016. 4
- [17] Alexander Hermans, Lucas Beyer, and Bastian Leibe. In defense of the triplet loss for person re-identification. *arXiv preprint arXiv:1703.07737*, 2017. 1, 2, 4
- [18] Jie Hu, Li Shen, and Gang Sun. Squeeze-and-excitation networks. In *Proceedings of the IEEE conference on computer vision and pattern recognition*, pages 7132–7141, 2018. 7
- [19] Rui Hu and John Collomosse. A performance evaluation of gradient field hog descriptor for sketch based image retrieval. *Computer Vision and Image Understanding*, 117(7):790–806, 2013. 3
- [20] Jay J Jiang and David W Conrath. Semantic similarity based on corpus statistics and lexical taxonomy. *arXiv preprint cmp-lg/9709008*, 1997. 3
- [21] Diederik P Kingma and Jimmy Ba. Adam: A method for stochastic optimization. *arXiv preprint arXiv:1412.6980*, 2014. 7
- [22] Elyor Kodirov, Tao Xiang, and Shaogang Gong. Semantic autoencoder for zero-shot learning. In *Proceedings of the IEEE conference on computer vision and pattern recognition*, pages 3174–3183, 2017. 6
- [23] Chenggang Li, Yinhao Wang, Zhicheng Zhao, and Fei Su. Vehicle re-identification: Logistic triplet embedding regularized by label smoothing. In *2019 IEEE Visual Communications and Image Processing (VCIP)*, pages 1–4. IEEE, 2019. 2
- [24] Jiangtong Li, Zhixin Ling, Li Niu, and Liqing Zhang. Bi-directional domain translation for zero-shot sketch-based image retrieval. *arXiv preprint arXiv:1911.13251*, 2019. 6
- [25] Li Liu, Fumin Shen, Yuming Shen, Xianglong Liu, and Ling Shao. Deep sketch hashing: Fast free-hand sketch-based image retrieval. In *Proceedings of the IEEE conference on computer vision and pattern recognition*, pages 2862–2871, 2017. 3, 6
- [26] Qing Liu, Lingxi Xie, Huiyu Wang, and Alan L Yuille. Semantic-aware knowledge preservation for zero-shot sketch-based image retrieval. In *Proceedings of the IEEE/CVF International Conference on Computer Vision*, pages 3662–3671, 2019. 2, 4, 6, 7
- [27] Weiyang Liu, Yandong Wen, Zhiding Yu, Ming Li, Bhiksha Raj, and Le Song. Sphered: Deep hypersphere embedding

- for face recognition. In *Proceedings of the IEEE conference on computer vision and pattern recognition*, pages 212–220, 2017. 1, 2
- [28] Ilya Loshchilov and Frank Hutter. Sgdr: Stochastic gradient descent with warm restarts. *arXiv preprint arXiv:1608.03983*, 2016. 7
- [29] Peng Lu, Gao Huang, Yanwei Fu, Guodong Guo, and Hangyu Lin. Learning large euclidean margin for sketch-based image retrieval. *arXiv preprint arXiv:1812.04275*, 2018. 2, 3, 4, 6, 7
- [30] Hao Luo, Youzhi Gu, Xingyu Liao, Shenqi Lai, and Wei Jiang. Bag of tricks and a strong baseline for deep person re-identification. In *Proceedings of the IEEE/CVF Conference on Computer Vision and Pattern Recognition Workshops*, pages 0–0, 2019. 2
- [31] Tomas Mikolov, Kai Chen, Greg Corrado, and Jeffrey Dean. Efficient estimation of word representations in vector space. *arXiv preprint arXiv:1301.3781*, 2013. 3
- [32] George A Miller. Wordnet: a lexical database for english. *Communications of the ACM*, 38(11):39–41, 1995. 3
- [33] Yair Movshovitz-Attias, Alexander Toshev, Thomas K Leung, Sergey Ioffe, and Saurabh Singh. No fuss distance metric learning using proxies. In *Proceedings of the IEEE International Conference on Computer Vision*, pages 360–368, 2017. 2
- [34] Hyun Oh Song, Yu Xiang, Stefanie Jegelka, and Silvio Savarese. Deep metric learning via lifted structured feature embedding. In *Proceedings of the IEEE conference on computer vision and pattern recognition*, pages 4004–4012, 2016. 2
- [35] Anubha Pandey, Ashish Mishra, Vinay Kumar Verma, Anurag Mittal, and Hema Murthy. Stacked adversarial network for zero-shot sketch based image retrieval. In *Proceedings of the IEEE/CVF Winter Conference on Applications of Computer Vision*, pages 2540–2549, 2020. 3
- [36] Omkar M Parkhi, Andrea Vedaldi, and Andrew Zisserman. Deep face recognition. 2015. 2
- [37] Adam Paszke, Sam Gross, Soumith Chintala, Gregory Chanan, Edward Yang, Zachary DeVito, Zeming Lin, Alban Desmaison, Luca Antiga, and Adam Lerer. Automatic differentiation in pytorch. 2017. 7
- [38] Jeffrey Pennington, Richard Socher, and Christopher D Manning. Glove: Global vectors for word representation. In *Proceedings of the 2014 conference on empirical methods in natural language processing (EMNLP)*, pages 1532–1543, 2014. 3
- [39] Qi Qian, Lei Shang, Baigui Sun, Juhua Hu, Hao Li, and Rong Jin. Softtriple loss: Deep metric learning without triplet sampling. In *Proceedings of the IEEE/CVF International Conference on Computer Vision*, pages 6450–6458, 2019. 2
- [40] A. S. Razavian, H. Azizpour, J. Sullivan, and S. Carlsson. Cnn features off-the-shelf: An astounding baseline for recognition. In *2014 IEEE Conference on Computer Vision and Pattern Recognition Workshops*, pages 512–519, 2014. 1
- [41] Scott Reed, Zeynep Akata, Honglak Lee, and Bernt Schiele. Learning deep representations of fine-grained visual descriptions. In *Proceedings of the IEEE conference on computer vision and pattern recognition*, pages 49–58, 2016. 1
- [42] Jose M Saavedra, Juan Manuel Barrios, and S Orand. Sketch based image retrieval using learned keyshapes (lks). In *BMVC*, volume 1, page 7, 2015. 3
- [43] Patsorn Sangkloy, Nathan Burnell, Cusuh Ham, and James Hays. The sketchy database: learning to retrieve badly drawn bunnies. *ACM Transactions on Graphics (TOG)*, 35(4):1–12, 2016. 3, 6
- [44] Florian Schroff, Dmitry Kalenichenko, and James Philbin. Facenet: A unified embedding for face recognition and clustering. In *Proceedings of the IEEE conference on computer vision and pattern recognition*, pages 815–823, 2015. 1, 2
- [45] Yuming Shen, Li Liu, Fumin Shen, and Ling Shao. Zero-shot sketch-image hashing. In *Proceedings of the IEEE Conference on Computer Vision and Pattern Recognition*, pages 3598–3607, 2018. 3, 6, 7
- [46] Kihyuk Sohn. Improved deep metric learning with multi-class n-pair loss objective. In *Proceedings of the 30th International Conference on Neural Information Processing Systems*, pages 1857–1865, 2016. 2
- [47] Yifan Sun, Changmao Cheng, Yuhan Zhang, Chi Zhang, Liang Zheng, Zhongdao Wang, and Yichen Wei. Circle loss: A unified perspective of pair similarity optimization. In *Proceedings of the IEEE/CVF Conference on Computer Vision and Pattern Recognition*, pages 6398–6407, 2020. 2
- [48] Yifan Sun, Liang Zheng, Weijian Deng, and Shengjin Wang. Svdnet for pedestrian retrieval. In *Proceedings of the IEEE International Conference on Computer Vision*, pages 3800–3808, 2017. 1
- [49] Yaniv Taigman, Ming Yang, Marc’ Aurelio Ranzato, and Lior Wolf. Deepface: Closing the gap to human-level performance in face verification. In *Proceedings of the IEEE conference on computer vision and pattern recognition*, pages 1701–1708, 2014. 1, 2
- [50] Laurens Van der Maaten and Geoffrey Hinton. Visualizing data using t-sne. *Journal of machine learning research*, 9(11), 2008. 13
- [51] Feng Wang, Jian Cheng, Weiyang Liu, and Haijun Liu. Additive margin softmax for face verification. *IEEE Signal Processing Letters*, 25(7):926–930, 2018. 1, 2
- [52] Feng Wang, Xiang Xiang, Jian Cheng, and Alan Loddon Yuille. Normface: L2 hypersphere embedding for face verification. In *Proceedings of the 25th ACM international conference on Multimedia*, pages 1041–1049, 2017. 1, 2
- [53] Hao Wang, Yitong Wang, Zheng Zhou, Xing Ji, Dihong Gong, Jingchao Zhou, Zhifeng Li, and Wei Liu. Cosface: Large margin cosine loss for deep face recognition. In *Proceedings of the IEEE conference on computer vision and pattern recognition*, pages 5265–5274, 2018. 1, 2
- [54] Jian Wang, Feng Zhou, Shilei Wen, Xiao Liu, and Yuanqing Lin. Deep metric learning with angular loss. In *Proceedings of the IEEE International Conference on Computer Vision*, pages 2593–2601, 2017. 2
- [55] Xun Wang, Xintong Han, Weilin Huang, Dengke Dong, and Matthew R Scott. Multi-similarity loss with general pair weighting for deep metric learning. In *Proceedings of the IEEE/CVF Conference on Computer Vision and Pattern Recognition*, pages 5022–5030, 2019. 2

- [56] Kilian Q Weinberger, John Blitzer, and Lawrence K Saul. Distance metric learning for large margin nearest neighbor classification. In *Advances in neural information processing systems*, pages 1473–1480, 2006. [2](#)
- [57] Yang Yang, Yadan Luo, Weilun Chen, Fumin Shen, Jie Shao, and Heng Tao Shen. Zero-shot hashing via transferring supervised knowledge. In *Proceedings of the 24th ACM international conference on Multimedia*, pages 1286–1295, 2016. [3](#), [6](#)
- [58] Sasi Kiran Yelamarthi, Shiva Krishna Reddy, Ashish Mishra, and Anurag Mittal. A zero-shot framework for sketch based image retrieval. In *Proceedings of the European Conference on Computer Vision (ECCV)*, pages 300–317, 2018. [2](#), [3](#), [6](#), [7](#), [8](#)
- [59] Qian Yu, Feng Liu, Yi-Zhe Song, Tao Xiang, Timothy M Hospedales, and Chen-Change Loy. Sketch me that shoe. In *Proceedings of the IEEE Conference on Computer Vision and Pattern Recognition*, pages 799–807, 2016. [3](#)
- [60] Qian Yu, Yongxin Yang, Feng Liu, Yi-Zhe Song, Tao Xiang, and Timothy M Hospedales. Sketch-a-net: A deep neural network that beats humans. *International journal of computer vision*, 122(3):411–425, 2017. [3](#)
- [61] Hua Zhang, Si Liu, Changqing Zhang, Wenqi Ren, Rui Wang, and Xiaochun Cao. Sketchnet: Sketch classification with web images. In *Proceedings of the IEEE conference on computer vision and pattern recognition*, pages 1105–1113, 2016. [3](#), [6](#)
- [62] Jingyi Zhang, Fumin Shen, Li Liu, Fan Zhu, Mengyang Yu, Ling Shao, Heng Tao Shen, and Luc Van Gool. Generative domain-migration hashing for sketch-to-image retrieval. In *Proceedings of the European conference on computer vision (ECCV)*, pages 297–314, 2018. [3](#)
- [63] Xiaofan Zhang, Feng Zhou, Yuanqing Lin, and Shaoting Zhang. Embedding label structures for fine-grained feature representation. In *Proceedings of the IEEE Conference on Computer Vision and Pattern Recognition*, pages 1114–1123, 2016. [1](#)
- [64] Yuting Zhang, Xueming Qian, Xianglong Tan, Junwei Han, and Yuanyan Tang. Sketch-based image retrieval by salient contour reinforcement. *IEEE Transactions on Multimedia*, 18(8):1604–1615, 2016. [3](#)
- [65] Zhaolong Zhang, Yuejie Zhang, Rui Feng, Tao Zhang, and Weiguo Fan. Zero-shot sketch-based image retrieval via graph convolution network. In *Proceedings of the AAAI Conference on Artificial Intelligence*, volume 34, pages 12943–12950, 2020. [2](#), [3](#), [6](#), [7](#)
- [66] Jiawen Zhu, Xing Xu, Fumin Shen, Roy Ka-Wei Lee, Zheng Wang, and Heng Tao Shen. Ocean: A dual learning approach for generalized zero-shot sketch-based image retrieval. In *2020 IEEE International Conference on Multimedia and Expo (ICME)*, pages 1–6. IEEE, 2020. [2](#), [3](#), [6](#), [7](#)

Appendix A.

A.1. Implementation details of GAN

The objective of generator G and discriminator D is written as:

$$\begin{aligned} \mathcal{L}_{adv-D}(G, D, S, P) = & \mathbb{E}_{p \sim p_{data}(p)} [\log (D(G(p)))] \\ & + \mathbb{E}_{s \sim p_{data}(s)} [\log (1 - D(G(s)))] \end{aligned} \tag{14}$$

$$\begin{aligned} \mathcal{L}_{adv-G}(G, D, S, P) = & \mathbb{E}_{p \sim p_{data}(p)} [\log (1 - D(G(p)))] \\ & + \mathbb{E}_{s \sim p_{data}(s)} [\log (D(G(s)))] \end{aligned} \tag{15}$$

where S is the input sketches and P is the input photos. The \mathcal{L}_{adv-D} teaches the discriminator D to make the right predictions on the modality of input feature, while the \mathcal{L}_{adv-G} encourages D to produce the wrong prediction by updating generator G . During each iteration, we fix D and update G with \mathcal{L}_{all} (Eq. 1) and \mathcal{L}_{adv-G} at first, then freeze G and update D with \mathcal{L}_{adv-D} . By optimizing G and D with \mathcal{L}_{adv-G} and \mathcal{L}_{adv-D} iteratively, the generator tends to produce features that have similar distribution for input sketches and photos.

A.2. Hyper-parameter Analysis

We analyze the effect of hyper-parameter λ on the TU-Berlin Extension dataset. Setting λ to 0 means the model is trained without the embedding loss. Table 4 shows that mAP@all and Prec@100 scores reach a peak value when $\lambda = 1.0$. Thus we set λ to 1.0 in all the other experiments.

Table 4. The mAP@all and Prec@100 results on the TU-Berlin Extension dataset with different λ .

λ	mAP@all	Prec@100
0.0	46.00 \pm 0.16	56.42 \pm 0.18
0.5	49.98 \pm 0.19	60.12 \pm 0.25
1.0	50.82 \pm 0.12	60.62 \pm 0.18
1.5	50.58 \pm 0.33	60.50 \pm 0.39
2.0	50.58 \pm 0.27	60.30 \pm 0.35
2.5	50.36 \pm 0.19	60.00 \pm 0.24
3.0	50.38 \pm 0.17	60.10 \pm 0.29

A.3. Qualitative Analysis

Visualization of Feature Embedding We visualize the 512-d feature extracted by our baseline model and the full model on the test set of TU-Berlin Extension in Figure 6. The feature representation of our MATHM is well clustered by categories. In contrast, our baseline model results show a large modality gap between samples with different modalities of the same category. The visualization is consistent with our qualitative analysis, which validates that MATHM resolves the problem of modality discrepancy better than our baseline.

Visualization of Retrievals Figure 7 shows the Top-10 retrieval results obtain by our full model on the TU-Berlin Extension dataset. Our model successfully retrieves photo images with the correct category label in most cases. We also present some negative cases where our model fails to retrieve photos with the same category as the query sketch. These wrongly retrieved images usually share some salient visual component to the ground truth categories, *e.g.*, both the *fan* and *windmill* contain three pieces of blades while the *laptop* and *telephone* have a similar keyboard. If we add a circle on the boundary of the sketch *fan*, as “fan-1” in Figure 7 shows, the retrieval accuracy dramatically increases. This important observation implies that our model has learned a shared embedding space for inputs from both sketches and photos. The failure of retrieval is mainly due to the inter-class similarity of sketches from certain categories.

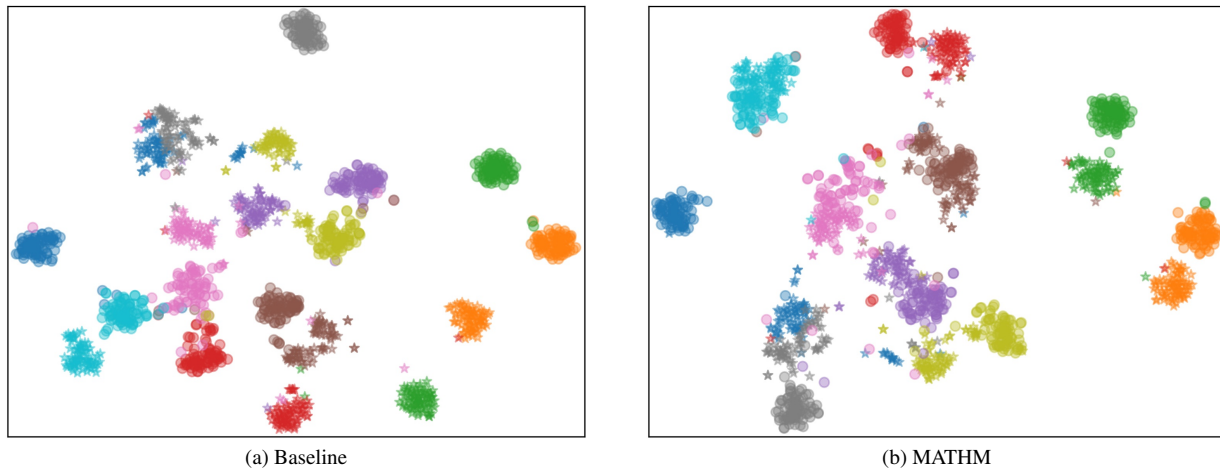


Figure 6. The t-SNE [50] visualization of the feature representation on ten randomly chosen classes from the testing set of TU-Berlin Extension. (a) and (b) show the features extracted by our baseline and MATHM, respectively. Each color represents a particular class. The stars denote sketches, and circles denote photos. Best viewed in color.



Figure 7. Top-10 retrieval results of our full model on TU-Berlin Extension. The correct results are in green, while the wrong results are in red. Best viewed in color.